



Cite this: *Dalton Trans.*, 2016, **45**, 1998

Received 20th July 2015,
Accepted 28th August 2015

DOI: 10.1039/c5dt02757h

www.rsc.org/dalton

Synthetic strategies to bicyclic tetraphosphanes using P₁, P₂ and P₄ building blocks†

Jonas Bresien,^a Kirill Faust,^a Christian Hering-Junghans,^a Julia Rothe,^a Axel Schulz^{*a,b} and Alexander Villinger^a

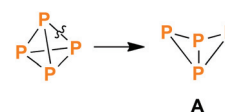
Different reactions of Mes* substituted phosphanes (Mes* = 2,4,6-tri-*tert*-butylphenyl) led to the formation of the bicyclic tetraphosphane Mes*P₄Mes* (**5**) and its unknown Lewis acid adduct **5**·GaCl₃. In this context, the *endo*–*exo* isomer of **5** was fully characterized for the first time. The synthesis was achieved by reactions involving “self-assembly” of the P₄ scaffold from P₁ building blocks (*i.e.* primary phosphanes) or by reactions starting from P₂ or P₄ scaffolds (*i.e.* a diphosphene or cyclic tetraphosphane). Furthermore, interconversion between the *exo*–*exo* and *endo*–*exo* isomer were studied by ³¹P NMR spectroscopy. All compounds were fully characterized by experimental as well as computational methods.

Introduction

Ring systems composed of group 15 elements (pnictogens, Pn) are an intriguing and widely investigated aspect of main group chemistry.^{1–3} Within this field of research, the chemistry of phosphorus based ring systems has become an important branch of inorganic chemistry,^{4,5} especially in view of the fact that various phosphorus ring systems can be obtained by direct activation of white phosphorus.^{6–8} A lot of work has been carried out to improve the selectivity of these activation processes, involving functionalization of P₄ by Lewis acids and bases, (transition) metals, radicals, or singlet carbenes such as N-heterocyclic carbenes (NHCs) or cyclic alkylaminocarbenes (CAACs).^{9–12}

Among a plethora of structural motifs found in phosphorus ring systems, the simple tetraphosphabicyclo[1.1.0]butane scaffold (**A**, Scheme 1) is of special interest. Firstly, it can formally be derived from tetrahedral P₄ by “simple” cleavage of one PP bond. Secondly, and more importantly, tetraphosphabicyclo[1.1.0]butanes were indeed obtained by P₄ activation, thus representing worthwhile target molecules in phosphorus chemistry.

The first tetraphosphabicyclo[1.1.0]butane, (Me₃Si)₂N–P₄–N(SiMe₃)₂ (**1a**, **1b**, Scheme 2), was synthesized by the group of



Scheme 1 Breaking one of the PP bonds in tetrahedral P₄ formally yields the tetraphosphabicyclo[1.1.0]butane scaffold (**A**).

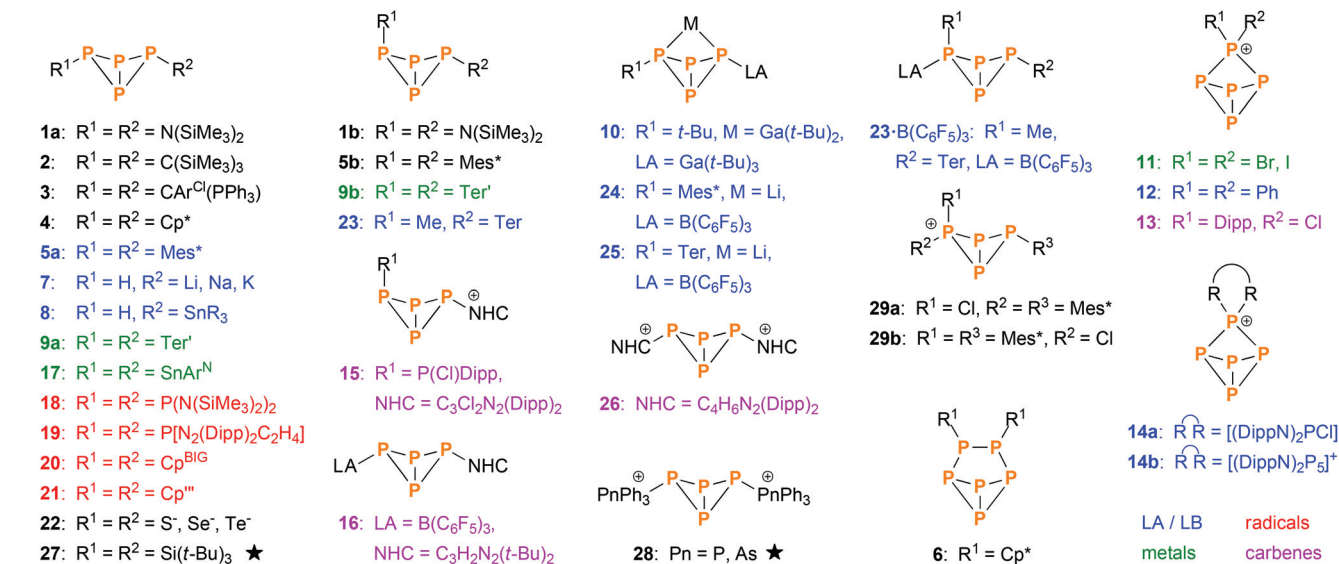
Niecke in 1982.¹³ It was derived from P₂ building blocks utilizing PP coupling reactions. In the following years, some more examples emerged that were derived from P₂ or P₃ units, as reported by Cowley (**2**),¹⁴ Schmidpeter (**3**),¹⁵ Jutzi (**4–6**),^{16–19} Weber (**5a**),²⁰ and Romanenko (**5a**).²¹ However, the majority of bicyclic tetraphosphanes was synthesized by P₄ activation, the first example being *exo*–*exo*–Mes*P₄Mes* (**5a**, Mes* = 2,4,6-tri-*tert*-butylphenyl), which was reported by Fluck and co-workers in 1985.^{22,23} Improvement of P₄ activation methods led to various other bicyclic P₄ species, which can be categorized by the aforementioned types of P₄ activation (Scheme 2); important contributions were made by the groups of Baudler (**7**, **8**),^{24,25} Power (**9–10**),^{26,27} Krossing (**11**),²⁸ Weigand (**12–15**),^{29,30} Tamm (**16**),³¹ Roesky and Stalke (**17**),³² Lappert (**18**),³³ Masuda (**19**),³⁴ Scheer (**20**, **21**),¹⁰ Karaghiosoff (**22**),³⁵ Lammertsma (**23–25**),¹² and Jones (**26**).³⁶ Additionally, various examples of transition metal complexes that incorporate bicyclic P₄ scaffolds were reported.^{11,37–42} In contrast, very few examples of self-assembly reactions exist (*i.e.* the bicyclic P₄ scaffold is built from P₁ building blocks in a single reaction); literature reports include Wiberg's (*t*-Bu)₃Si–P₄–Si(*t*-Bu)₃ (**27**)⁴³ and Weigand's [Ph₃Pn–P₄–PnPh₃]²⁺ (**28**, Pn = P, As).⁴⁴ Just recently, we reported on the cation [Mes*P₄(Cl)Mes*]⁺ (**29**),⁴⁵ which in itself was not derived by a self-assembly reaction, but its cyclic P₄ precursor was.⁴⁶

^aInstitut für Chemie, Universität Rostock, Albert-Einstein-Straße 3a, D-18059 Rostock, Germany. E-mail: axel.schulz@uni-rostock.de

^bLeibniz-Institut für Katalyse e.V. an der Universität Rostock, Albert-Einstein-Straße 29a, D-18059 Rostock, Germany

†Electronic supplementary information (ESI) available: Experimental and computational details, crystallographic and spectroscopic data. CCDC 1413820–1413827. For ESI and crystallographic data in CIF or other electronic format see DOI: 10.1039/c5dt02757h





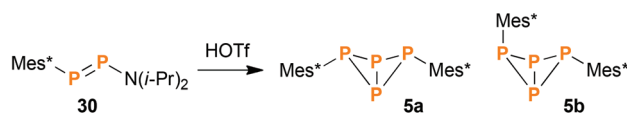
Scheme 2 Overview of known bicyclic tetraphosphane species (not including transition metal complexes). Most were synthesized by direct activation of P_4 using Lewis acids and bases (blue), metals or metal fragments (green), radical species (red) or singlet carbenes (violet). The rest was derived from other precursors, mainly P_2 and P_4 building blocks. Species indicated by a star were derived directly from P_1 building blocks in a self-assembly reaction. $\text{Ar}^{\text{Cl}} = 2,6\text{-dichlorophenyl}$; $\text{Ar}^{\text{N}} = \text{C}_6\text{H}_3\text{-}2,6\text{-}(\text{C}(\text{NDipp})\text{CH}_3)_2$; $\text{Cp} = \text{cyclopentadienyl}$; $\text{Cp}^* = \text{pentamethyl-Cp}$; $\text{Cp}^{\text{'''}} = 2,3,5\text{-tri-}t\text{-butyl-Cp}$; $\text{Cp}^{\text{BIG}} = \text{pentakis}(4\text{-}n\text{-butylphenyl})\text{-Cp}$; $\text{Dipp} = 2,6\text{-diisopropylphenyl}$; $\text{SnR}_3 = \text{SnMe}_3, \text{SnPh}_3, \text{Sn}(c\text{-Hex})_3$ or $\text{Sn}(o\text{-Tol})_3$; $\text{Ter} = 2,6\text{-dimesitylphenyl}$; $\text{Ter}^* = 2,6\text{-bis}(\text{diisopropylphenyl})\text{phenyl}$; $\text{LA} = \text{Lewis acid}$, $\text{LB} = \text{Lewis Base}$, $\text{NHC} = \text{N-heterocyclic carbene}$.

Interestingly, *exo-exo*-substituted tetraphosphabicyclo-[1.1.0]butanes are considerably more common than their *endo-exo*-substituted counterparts, indicating that the latter are energetically less favoured. We therefore took interest in the synthesis and characterization of rare *endo-exo*-substituted derivatives, which could be synthesized from P_1 , P_2 and P_4 building blocks and were analysed by experimental and computational methods.

Results and discussion

Synthesis and characterization of *endo-exo*- $\text{Mes}^*\text{P}_4\text{Mes}^*$ (**5b**)

During our research in functionalized *cyclo*-tetraphosphanes,⁴⁶ we came across a publication of Romanenko *et al.*,²¹ wherein the authors described the synthesis of *exo-exo*- $\text{Mes}^*\text{P}_4\text{Mes}^*$ (**5a**) and the asymmetrically substituted bicyclic system $\text{Mes}^*\text{P}_4\text{N}(i\text{-Pr})_2$ by reacting the diphosphene $\text{Mes}^*\text{PPN}(i\text{-Pr})_2$ (**30**) with equimolar amounts of HOTf ($\text{Tf} = \text{SO}_2\text{CF}_3$). Intrigued by this curious method to synthesize bicyclic tetraphosphanes, we tried to reproduce the experiment described in the publication. However, fractional crystallization of the product mixture did not yield the reported compound $\text{Mes}^*\text{P}_4\text{N}(i\text{-Pr})_2$, but rather *endo-exo*- $\text{Mes}^*\text{P}_4\text{Mes}^*$ (**5b**, Scheme 3), alongside the known product **5a** and minor amounts of the diphosphene $\text{Mes}^*\text{PPMes}^*$ (**31**).^{47,48} Probably the available NMR and MS data were misinterpreted in the original publication. Compound **5b** was now fully characterized for the first time, including NMR, Raman and IR spectroscopy, mass spectrometry, and single crystal X-ray diffraction.



Scheme 3 Reaction of diphosphene **30** with HOTf, yielding bicyclic phosphanes **5a** and **5b** as main products.

Spectroscopic characterization

Apart from minor impurities, the ^{31}P NMR spectrum of the reaction mixture showed an A_2X_2 ($-273.2, -128.3$ ppm) and an A_2MX spin system ($-220.4, -94.8, -54.7$ ppm) in a ratio of 1 : 4. The former set of signals was assigned to **5a** (17% yield based on ^{31}P NMR integrals), the latter to **5b** (67%); hence, the *endo-exo*-isomer was actually formed in significant excess. The same NMR data were obtained for pure **5a** and **5b** (Fig. 1), which agree well with calculated NMR shifts and coupling constants (ESI^+) as well as previously reported NMR data.^{17,22} Moreover, both isomers could be nicely distinguished in the Raman spectrum due to different excitation energies of the vibrational “breathing” mode of the P_4 scaffold (Table 1). The corresponding Raman bands were easily identified as the most intense signals in both spectra (**5a**: 592 cm^{-1} , **5b**: 568 cm^{-1}). The wavenumbers compare well to the symmetrical A_1 mode of tetrahedral P_4 in the gas phase (600 cm^{-1}).⁴⁹ In case of **5b**, two distinct P–C valence modes were identified at 584 (*exo*) and 591 cm^{-1} (*endo*). In **5a**, the single P–C valence band was superimposed by the “breathing” mode of the bicyclic scaffold and could not be discerned.



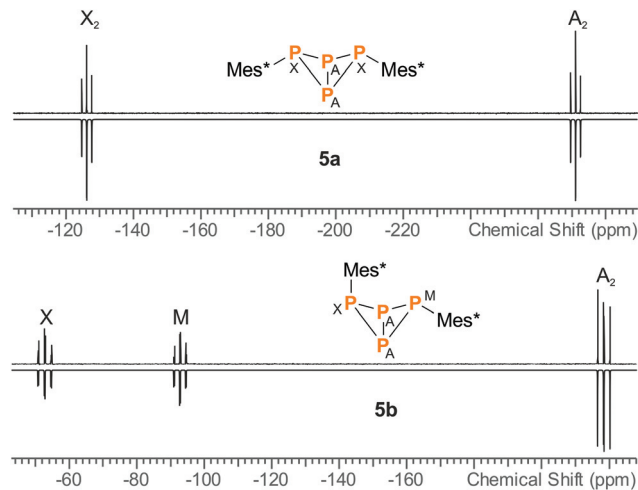


Fig. 1 Experimental (up) and simulated (down) ^{31}P NMR spectra of **5a** and **5b**.

Molecular structure

Crystallization from *n*-hexane yielded single crystals of **5b** in the space group $P\bar{1}$ while crystallization from CH_2Cl_2 afforded crystals in the space group $P2_1/n$ (Fig. 2, right). The P–P and P–C bond lengths are similar in both modifications of **5b**: the P1–P2 and P1–P3 bonds (av. 2.227, 2.233 Å) are close to the sum of the covalent radii ($\sum r_{\text{cov}} = 2.22$ Å),⁵⁰ whereas the P2–P4 and P3–P4 bonds (av. 2.213, 2.210 Å) as well as the transannular bond P2–P3 (av. 2.177 Å) are slightly shorter. This is in contrast to the structure of the previously reported *exo-exo*-isomer **5a** (Fig. 2, left),²² where all four peripheral P–P bonds exhibit similar lengths (av. 2.225 Å); the transannular bond, however,

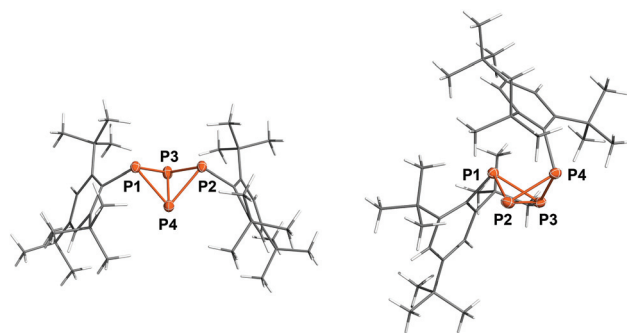


Fig. 2 Molecular structure of **5a** (left) and **5b** (monoclinic, right). Ellipsoids are set at 50% probability (173 K). Selected bond lengths [Å] and angles [°]: **5a** P1–P3 2.2310(7), P1–P4 2.2171(7), P2–P3 2.2294(7), P2–P4 2.2236(7), P3–P4 2.1634(8); P1–P3–P4–P2 $-95.66(3)^\circ$; **5b** P1–P2 2.2244(7), P1–P3 2.2326(8), P2–P4 2.2131(8), P3–P4 2.2101(8), P2–P3 2.1773(8); P1–P2–P3–P4 $107.78(3)^\circ$.

is likewise only 2.1634(8) Å. The bond angles at the P atoms are all close to 60° and thus compare to tetrahedral P_4 . Interestingly, the Mes* substituent in **5b** is bent backwards above the P_4 scaffold, so the *p-tert*-butyl group rests on top of the *exo*-Mes* substituent, effectively shielding the top side of the bicyclic ring system. Hence, the fold angle of the butterfly-shaped P_4 scaffold is quite different in all three cases; it varies from $95.66(3)^\circ$ (**5a**) across $105.75(5)^\circ$ (triclinic **5b**) to $107.78(3)^\circ$ (monoclinic **5b**), which can be attributed to Pauli repulsion between the *endo*-substituent and the opposite bridging atom (P1) in case of **5b** as well as packing effects to account for the difference between the two modifications. A similar effect was observed in case of $\text{Ter}'\text{P}_4\text{Ter}'$ (**9a**, **9b**, $\text{Ter}' = 2,6\text{-bis}(\text{diisopropylphenyl})\text{phenyl}$), where the difference between *exo-exo* (92.9°) and *endo-exo*-isomer (108.1°) is even larger.²⁷

Table 1 Main vibrational modes of bicyclic tetraphosphanes in the Raman spectrum. Assignment of the symmetries based on approximate C_{2v} symmetry of the P_4 scaffold

Vibration mode	Description	Frequency [cm^{-1}]
	Symmetrical valence “breathing mode” (A_1 mode, in phase)	5a : 592 5b : 568 5a-GaCl₃ : 597 5b-GaCl₃ : 567
	Peripheral bond stretch (B_1 mode)	5a : 447 5b : 500 5a-GaCl₃ : 497 5b-GaCl₃ : 518
	Transannular bond stretch (A_1 mode, out of phase)	5a : 412 5b : — 5a-GaCl₃ : 436 5b-GaCl₃ : —
	Peripheral bond stretch (B_2 mode)	5a : 412 5b : 412 5a-GaCl₃ : 451 5b-GaCl₃ : 438



Computational study

Comprehensive DFT calculations were carried out to compare the isomers **5a** and **5b**. According to NBO analysis,⁵¹ the bonding situation is similar in both cases. The Wiberg and NLMO bond indices are near unity for all P–P bonds. However, due to the small bond angles, the electron density is not distributed symmetrically around the P–P bond axes, but rather bent outwards, resulting in banana-shaped bonds. This is illustrated by the electron localization function (ELF, Fig. 3 right), where the local maxima between the P atoms are found outside the lines of nuclear centres. Additionally, the symmetry and shape of the natural bond orbitals (NBOs) and molecular orbitals (MOs) support this picture.

Isomerization of **5b** to **5a**

At the PBE0/aug-cc-pVDZ level of theory, the *exo-exo*-isomer **5a** is energetically favoured with respect to **5b** by 10.4 kJ mol⁻¹ (ΔH^{298}) or 8.80 kJ mol⁻¹ (ΔG^{298}), respectively. These findings prompted us to investigate the thermodynamic equilibrium between both isomers: Indeed, when heating a THF solution of **5a** and **5b** (1 : 4 ratio) to 75 °C over a period of 50 days, slow conversion of **5b** to **5a** was observed in the ³¹P NMR spectrum. The forward and backward reaction were modelled as first order kinetics according to eqn (1).



Hence, eqn (2) defines the reaction rate, $[\mathbf{5a}]$ and $[\mathbf{5b}]$ being the partial concentrations of **5a** and **5b**, respectively.

$$\frac{d[\mathbf{5b}]}{dt} = -k_f[\mathbf{5b}] + k_b[\mathbf{5a}] \quad (2)$$

Let $[\mathbf{5a}]_0$ and $[\mathbf{5b}]_0$ denominate the initial concentrations at $t = 0$. Due to the conservation of mass, $[\mathbf{5b}]_0 - [\mathbf{5b}]$ equals

$[\mathbf{5a}] - [\mathbf{5a}]_0$. Furthermore, the reaction rate becomes zero at equilibrium, when the system reaches a steady state with constant concentrations of both isomers. Using these boundary conditions to integrate eqn (2), we obtain

$$[\mathbf{5b}] = c + ([\mathbf{5b}]_0 - c)e^{-(k_f+k_b)t} \quad (3)$$

$$c = \frac{k_b}{k_f + k_b} ([\mathbf{5a}]_0 + [\mathbf{5b}]_0) \quad (4)$$

Least-squares fitting of eqn (3) against the experimentally determined concentrations gave $k_f = 2.77(11) \times 10^{-6} \text{ s}^{-1}$ and $k_b = 0.30(3) \times 10^{-6} \text{ s}^{-1}$. Accordingly, the experimental equilibrium constant is:

$$K = \frac{k_f}{k_b} = 9.3(1.4) \quad (5)$$

Thus, the experimental Gibbs energy (at 75 °C) can be calculated:

$$\Delta_R G = -RT \ln K = -6.4(3) \text{ kJ mol}^{-1} \quad (6)$$

This value compares well to the calculated value of $\Delta_R G^{348} = -8.54 \text{ kJ mol}^{-1}$ for the gas phase reaction.

Intriguingly, an equilibrium between *endo-exo* and *exo-exo*-isomers was also described for Ter'P₄Ter' (**9a**, **9b**); however, the system was found to be highly dynamic and both isomers afforded identical NMR spectra even at low temperature. Crystallization of either one of the isomers depended solely on the solvent used.²⁷

Synthesis of *endo-exo*-Mes*P₄Mes* (**5b**) by carbene promoted degradation of [CIP(μ-PMes*)]₂ (**32**)

Using the synthetic protocol described above, **5a** and **5b** were always obtained in mixture. Separation was difficult and could only be achieved for small amounts of substance by repeated re-crystallization. Designing a reaction that would yield **5b**

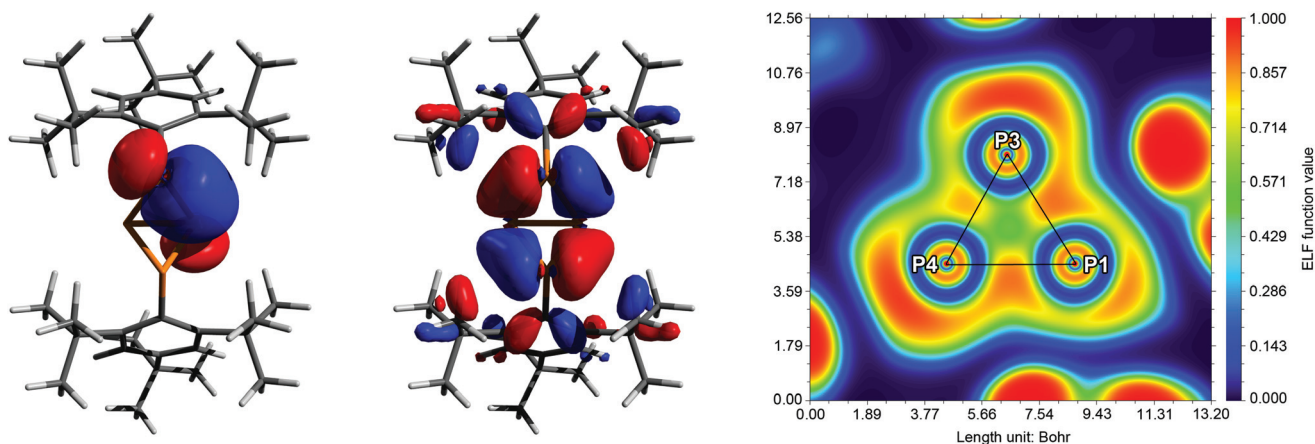
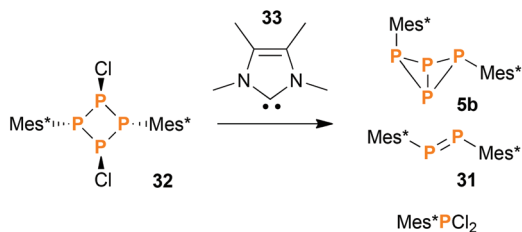


Fig. 3 Exemplary description of the bonding in **5a**. Left: NBO/NLMO depiction of one PP bond, illustrating the “banana” bond character. Middle: HOMO–6 with large coefficients at the central P₄ scaffold. Right: Electron localization function (ELF) depicted in a plane through atoms P1, P3 and P4. The maximum densities between the P atoms are found outside the lines of nuclear centres (black). The maxima at the corners of the triangle show the location of the lone pairs (LPs).



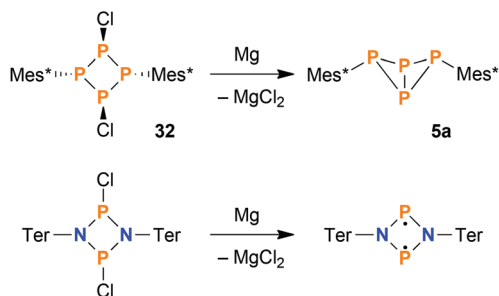


Scheme 4 The carbene promoted degradation of **32** yields a mixture of products, of which some were identified.

exclusively proved to be difficult: obviously, all reactions involving elevated temperatures led to (at least) partial formation of the thermodynamically favoured *exo-exo*-isomer **5a**. Still, we found that the reaction of the *cyclo*-tetraphosphane $[\text{ClP}(\mu\text{-PMes}^*)_2]$ (**32**)⁴⁶ with tetramethylimidazolyliene (**33**) yielded bicyclic tetraphosphane **5** in a surprisingly good isomeric ratio (**5a** : **5b**) of 1 : 12 (Scheme 4). The isolated yield of pure **5b** was low (14% based on **32**), since the degradation of **32** did not proceed cleanly but rather gave a mixture of different products. Anyway, **5b** could be crystallized from the reaction mixture in large, block-shaped crystals, making isolation comparatively easy.

Selective synthesis of *exo-exo*-Mes*P₄Mes* (**5a**) by reduction

Concerning the synthesis of pure **5a**, the isomerisation at elevated temperatures certainly offered a viable possibility to increase the isomeric ratio in favour of the *exo-exo* isomer. Nevertheless, we found a much more straightforward way to synthesize pure **5a**: starting from **32**, reduction with stoichiometric amounts of Mg afforded **5a** in high yields (based on ³¹P NMR integrals: 95%; isolated substance: 73%) in a clean reaction (Scheme 5, top). For comparison, the original synthesis of **5a** published by Fluck *et al.* afforded the bicyclic phosphane in a yield of only 5.2%.²² Formally, the reduction of **32** with Mg can be compared to the reduction of dichloro-*cyclo*-diphosphadiazanes, $[\text{ClP}(\mu\text{-NR})_2]$, which results in the formation of *cyclo*-diphosphadiazanediyls, $[\text{P}(\mu\text{-NR})_2]$, provided that the substituent R is bulky enough to prevent dimerization (Scheme 5,



Scheme 5 Top: Reduction of *cyclo*-tetraphosphane **32** yields bicyclic phosphane **5a** selectively. Bottom: Reduction of homologous dichloro-*cyclo*-diphosphadiazanes results in singlet open-shell biradicals with a drastically different bonding situation.

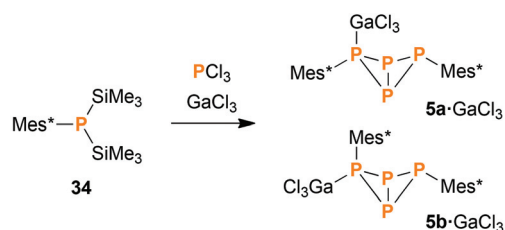
bottom).⁵² Yet, in contrast to the bicyclic tetraphosphane, the NP species comprise a planar ring system with singlet bi-radical character, as there is no classical bonding interaction between the transannular P atoms in this case.

Synthesis of Mes*P₄Mes*·GaCl₃ (**5**·GaCl₃) from P₁ units

When heating a solution of Mes*P(SiMe₃)₂ (**34**) in the presence of PCl₃, a mixture of various products was obtained. Interestingly, the *exo-exo*-isomer **5a** was found to be one of the major products. Other species that could be identified were Mes*PPMes* (**31**), Mes*PCl₂, P₄, *endo-exo*-isomer **5b** (minor amounts), and some higher aggregates of uncertain composition. However, the reaction was rather slow, so we decided to add a Lewis acid for activation purposes. Indeed, in the presence of GaCl₃, complete conversion was detected after one hour even at low temperatures (Scheme 6). Upon slow warming to ambient temperature, colourless crystals of **5a**·GaCl₃ or **5b**·GaCl₃ were obtained. Depending on the solvent, either one could be crystallized selectively, even though the ratio of both isomers in solution (7 : 5) remained unaffected by the choice of solvent.

Spectroscopic characterization

For both **5a**·GaCl₃ and **5b**·GaCl₃, an A₂MX spin system was expected due to unsymmetrical substitution of the bicyclic scaffold. Nonetheless, the room temperature ³¹P NMR spectrum of **5a**·GaCl₃ only displayed two resonances (formal A₂X₂ pattern; −246.4, −97.1 ppm; Fig. 4), which were shifted downfield by *ca.* 30 ppm with respect to non-coordinating **5a**. At −80 °C, though, the actual A₂MX spin system was resolved (−248.1, −114.0, −74.8 ppm), with a rather large ²J_{MX} coupling constant of +225 Hz (*cf.* **5b**: ²J_{MX} = −27 Hz). To investigate the nature of this dynamic effect, temperature dependent NMR spectra were recorded. Basically, either an *intramolecular* or an *intermolecular* exchange (*i.e.* dissociation or bimolecular exchange) of the GaCl₃ unit could be responsible for the observed line shapes, given that the concentration of free **5a** is much lower than the concentration of the adduct **5a**·GaCl₃ (approx. ratio of 10^{−2} or less). However, at such low concentrations, the free phosphane could well be below the detection limit and it might not be discernible in the spectrum even at slow exchange. Accordingly, we added an excess of **5a**, so the appearance of the NMR spectrum would change drastically if the free phosphane (*i.e.* dissociation) was involved in the



Scheme 6 Reacting **34** with PCl₃ and GaCl₃ leads to GaCl₃ adducts of the bicyclic tetraphosphane **5**, among other products.



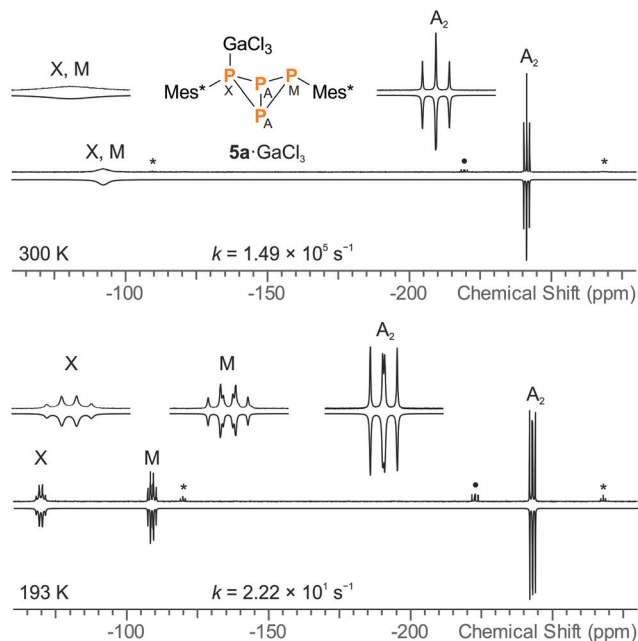


Fig. 4 Experimental (up) and simulated (down) ^{31}P NMR spectra of $5\text{a}\cdot\text{GaCl}_3$ at 27 °C (top) and -80 °C (bottom), demonstrating the dynamic exchange of the GaCl_3 moiety in solution (* = 5a , • = impurity of $5\text{b}\cdot\text{GaCl}_3$). GaCl_3 was added to 5a in slightly sub-stoichiometric amounts (0.95 eq.) so the non-coordinating bicyclic phosphane was detectable in the NMR spectrum.

observed exchange.⁵³ However, the signals of the excess phosphane could be detected independently of those of the adduct and the signal pattern of $5\text{a}\cdot\text{GaCl}_3$ remained unchanged, regardless of the excess of phosphane, proving an intramolecular mechanism (Scheme 7). Still, at higher temperatures above the coalescence of the M and X signal of $5\text{a}\cdot\text{GaCl}_3$, slight broadening of the signals of free 5a was detected, hinting at an independent intermolecular exchange. Full line-shape analysis of the NMR signals (Fig. 4, ESI†) facilitated derivation of the rate constants k at different temperatures. Using the Eyring eqn (7), the Gibbs energy of activation of the intramolecular exchange could be determined.

$$k = \kappa \frac{k_{\text{B}}T}{h} \exp\left(-\frac{\Delta G^\ddagger}{RT}\right) \quad (7)$$

Least-squares fitting gave a mean Gibbs energy of activation $\Delta G^\ddagger = 39.5(4) \text{ kJ mol}^{-1}$, which compares, for example, to the activation barrier of the exchange of NH_3 in $\text{H}_3\text{N}\cdot\text{GaMe}_3$



Scheme 7 In case of $5\text{a}\cdot\text{GaCl}_3$, a fast intramolecular exchange of the GaCl_3 unit was observed. The Gibbs energy of activation for this process was determined to be 39.5 kJ mol^{-1} .

(35.6 kJ mol^{-1}).⁵⁴ According to the linearized Eyring plot, the enthalpy of activation ΔH^\ddagger was found to be $39.5(4) \text{ kJ mol}^{-1}$ and the entropy of activation $\Delta S^\ddagger = -0.20(2) \text{ J mol}^{-1} \text{ K}^{-1}$, indicating a monomolecular transition state in agreement with the discussed intramolecular exchange reaction. The NMR data at slow exchange (-80 °C) correspond well with calculated NMR shifts and coupling constants (ESI†).

The *endo-exo* isomer $5\text{b}\cdot\text{GaCl}_3$ showed an A_2MX spin system (-224.5, -114.5, -50.0 ppm), which resembled the NMR spectrum of free 5b . Like in $5\text{a}\cdot\text{GaCl}_3$, the A part was broadened due to coupling with Ga. Owing to the arrangement of the Mes* substituents, no intramolecular exchange was observed; the linewidths did not change significantly upon cooling to -80 °C. Nonetheless, upon addition of an excess of 5b the ^{31}P NMR spectrum revealed a dynamic exchange between free phosphane and adduct, which is most likely caused by a bimolecular exchange of the type $5\cdot\text{GaCl}_3 + 5' \rightleftharpoons 5'\cdot\text{GaCl}_3 + 5$ (ESI†).

Both isomers were nicely distinguishable in the solid state Raman spectra, due to the different positions of the “breathing mode” bands, similar to the non-coordinating tetraphosphabicyclo[1.1.0]butanes 5a and 5b . In contrast to the latter, the most intense Raman signal was caused by the Ga-Cl stretching at 343 ($5\text{a}\cdot\text{GaCl}_3$) or 348 cm^{-1} ($5\text{b}\cdot\text{GaCl}_3$). P-C valence modes could be identified at 613 (Mes* at coordinating P, $5\text{a}\cdot\text{GaCl}_3$) and 618 cm^{-1} (*endo*-Mes*, $5\text{b}\cdot\text{GaCl}_3$), the other ones were superimposed by the intense “breathing mode” signals. Important vibrational modes of the P_4 scaffold are summarized in Table 1.

Molecular structure

Lewis acid adduct $5\text{a}\cdot\text{GaCl}_3$ crystallized in the orthorhombic space group $Pnma$ as *n*-hexane solvate (Fig. 5). The PP bond lengths lie within the range of typical single bonds, however the P3-P2 (or P3-P2') bond is slightly shortened (2.1805(9) Å); therefore, the bicyclic structure with two longer and two shorter bonds actually resembles the bicyclic scaffold in 5b .

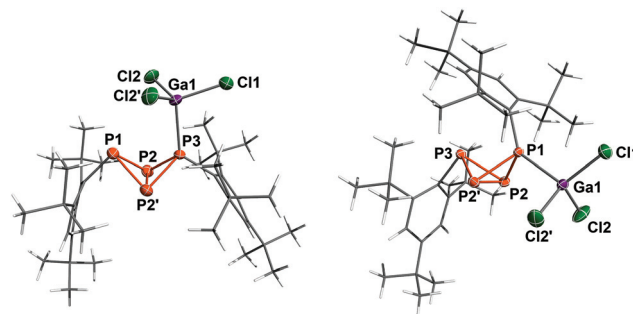


Fig. 5 Molecular structure of $5\text{a}\cdot\text{GaCl}_3$ (left) and $5\text{b}\cdot\text{GaCl}_3$ (right). Ellipsoids are set at 50% probability (173 K). Selected bond lengths [Å] and angles [°]: $5\text{a}\cdot\text{GaCl}_3$ P1-P2 2.228(1), P2-P3 2.1805(9), P2-P2' 2.200(1), Ga1-P3 2.4206(8), P1-P2-P2'-P3 98.96(3); $5\text{b}\cdot\text{GaCl}_3$ P1-P2 2.1854(5), P2-P3 2.2365(6), P2-P2' 2.2074(8), P1-Ga1 2.3966(5); P1-P2-P2'-P3 102.64(2).



The transannular bond (P2–P2': 2.200(1) Å), on the other hand, is noticeably longer than in **5a** or **5b**. In comparison with the sum of covalent radii (2.35 Å),⁵⁰ the P3–Ga1 bond is somewhat elongated (2.4206(8) Å), most likely due to Pauli repulsion between the *ortho-tert*-butyl groups of the neighbouring Mes* moiety and the GaCl₃ unit. The bonding angles at the coordinating P atom (P3) are considerably flattened, so one of the Mes* substituents is bent further outwards. Moreover, the fold angle of the bicyclic system amounts to 98.69(3)° and is therefore 3° larger than in **5a**.

Compound **5b**·GaCl₃ crystallized in the monoclinic space group *P*₂₁/*m* either as toluene or CH₂Cl₂ solvate with similar cell parameters and molecular structure. Hence only the toluene solvate shall be discussed in the following; again, the bonds between the bridgehead atoms and the coordinating P atom (P2–P1 and P2'–P1: 2.1854(5) Å) are shortened in comparison with **5b**, whereas the transannular bond is somewhat widened (P2–P2': 2.2074(8) Å). The P–Ga bond length (2.3699(5) Å) is shorter than in **5a**·GaCl₃ and compares well to the sum of covalent radii. The angle of the P3–P2–P2' plane to the P3–C13 bond axis (96.92(6)°) is about 8° smaller than in **5b**, so the Mes* substituent moves closer to the bicyclic scaffold. In contrast to **5a**·GaCl₃, the fold angle of **5b**·GaCl₃ lessens with respect to the free bicyclic tetraphosphane by 3° (102.64(2)°).

In both isomers, the substitution pattern at the bicyclic P₄ scaffold is comparable to the borane adduct TerP₄Me·B(C₆F₅)₃ (23-B(C₆F₅)₃) or the bicyclic phosphino-phosphonium cation [Mes*P₄(Cl)Mes*]⁺ (**29**).^{12,45}

Computational study

NBO analysis revealed that the partial charges of the P atoms in **5a**·GaCl₃ and **5b**·GaCl₃ (bridgehead P: +0.10*e*, coordinating P: +0.24*e*, non-coordinating P: +0.31*e*) changed only slightly in

comparison with **5a** and **5b** (bridgehead P: 0.00*e*, P(Mes*): +0.27*e*), implying a similar distribution of the electron density. Inspection of the molecular orbitals (MOs) showed that the principal bonding orbitals of the P₄ scaffold remained intact. According to the electron localization function (ELF), the P–Ga bond is strongly polarized towards phosphorus (Fig. 6). The natural Lewis description actually suggests a non-bonding situation with a lone pair (LP) at phosphorus and an empty p-type orbital at Ga, with low P–Ga bond indices (NLMO: 0.34, Wiberg: 0.50). However, a second order perturbation analysis revealed a strong donor–acceptor interaction between the LP at P and the empty p-type orbital at Ga (**5a**·GaCl₃: 530.5 kJ mol^{−1}, **5b**·GaCl₃: 555.2 kJ mol^{−1}); thus, the P–Ga bonding can be described as a classical dative bond. At the PBE0/aug-cc-pVDZ level of theory, the *exo-exo* isomer **5a**·GaCl₃ was calculated to be energetically favoured by 8.03 kJ mol^{−1} (Δ*G*²⁹⁸); therefore the energetic difference between *exo-exo* and *endo-exo*-isomer slightly decreased in comparison to non-coordinating **5a** and **5b**. This is reflected in the calculated Gibbs energies (Δ*RG*²⁹⁸) for the association of **5a** or **5b** and GaCl₃, which amount to −46.7 kJ mol^{−1} or −47.4 kJ mol^{−1}, respectively.

Equilibrium between **5a**·GaCl₃ and **5b**·GaCl₃

Similar to the free phosphanes, the GaCl₃ adducts **5a**·GaCl₃ and **5b**·GaCl₃ were found to interconvert slowly in solution at ambient temperature. Over a period of several weeks, the establishment of equilibrium was monitored by ³¹P NMR spectroscopy. Interestingly, the equilibrium constant was found to be 1.6(2), thus the amount of *endo-exo* isomer at equilibrium was significantly higher than in case of the free phosphanes. This is in agreement with the calculations, although the actual effect is even more pronounced. According to the experiment, the energetic difference between both isomers is just 1.2(4) kJ mol^{−1} (Δ*G*).

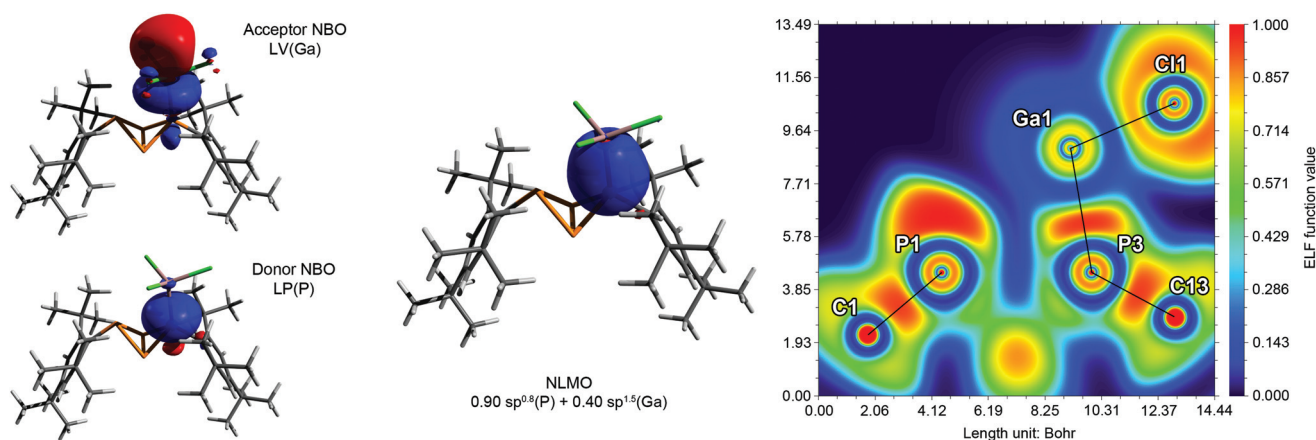
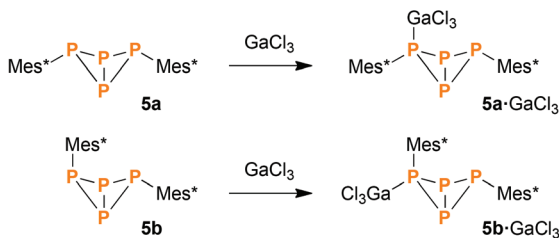


Fig. 6 Exemplary description of the bonding in **5a**·GaCl₃. Left: Donor and acceptor NBOs describing the dative bond from P to Ga. Middle: P–Ga bond in the natural localized MO (NLMO) picture. Right: Electron localization function (ELF) depicted in a plane through atoms P1, P3 and Ga1. The P–Ga and Ga–Cl bonds are strongly polarized and exhibit partly ionic character. The deformation of the LP at P1 is due to Pauli repulsion with C12 and C12' (out of plane).





Scheme 8 Rational synthesis of 5a·GaCl₃ and 5b·GaCl₃.

Direct synthesis of Mes*P₄Mes*·GaCl₃ (5·GaCl₃)

As expected, 5a·GaCl₃ and 5b·GaCl₃ could be synthesized from pure 5a and 5b by treatment with equimolar amounts of GaCl₃. Mixing solutions of both reactants and subsequent evaporation of the solvent led to quantitative yield of the respective GaCl₃ adduct (Scheme 8). Due to the short reaction time (*ca.* 5 min), isomerization could be avoided.

Conclusions

We present new insights into the chemistry of tetraphosphabicyclo[1.1.0]butanes: various synthetic approaches were investigated, involving precursor molecules with one, two or four phosphorus atoms. Thereby, the *endo-exo* isomer of Mes*P₄Mes* (5b) could be fully characterized for the first time and the interconversion of both isomers could be studied in detail. Furthermore, the hitherto unknown GaCl₃ adducts of both *exo-exo* and *endo-exo* isomer (5a·GaCl₃, 5b·GaCl₃) were thoroughly investigated, including experimental assessment of dynamic behaviour in solution and computational studies of the bonding situation.

Due to isomerization in solution, it is difficult to obtain either isomer purely; ideally, synthetic strategies should be designed to (a) minimize the reaction time and (b) take place at low temperatures to avoid thermodynamic equilibrium.

Experimental

All manipulations were carried out under oxygen- and moisture-free conditions under argon using standard Schlenk or Drybox techniques. All starting materials containing the Mes* moiety were synthesized according to modified literature procedures; other reactants and solvents were obtained from commercial sources and thoroughly dried. Detailed information concerning experimental procedures, data acquisition and processing, as well as purification of chemicals can be found in the ESI.†

Synthesis of 5a

A solution of [ClP(μ-PMes*)]₂ (206 mg, 0.30 mmol) in THF (3 mL) is added to magnesium turnings (10 mg, 0.42 mmol) and stirred at ambient temperature overnight. Subsequently,

the solvent is removed *in vacuo* and the solid residue is extracted with *n*-hexane (5 mL). After filtration, the filtrate is concentrated and stored at 5 °C, resulting in crystallization of colourless *exo-exo*-Mes*P₄Mes*. Yield: 135 mg (0.22 mmol, 73%). CHN calc. (found) in %: C 70.34 (70.32), H 9.51 (9.35). ³¹P{¹H} NMR (CD₂Cl₂, 121.5 MHz): δ = -273.2 (t, ¹J_{AX}(³¹P,³¹P) = -177 Hz, 2 P, P_{bridgehead}), -128.3 (t, ¹J_{AX}(³¹P,³¹P) = -177 Hz, 2 P, PMes*). ¹H NMR (CD₂Cl₂, 300.1 MHz): δ = 1.19 (s, 18 H, *p-t*-Bu), 1.63 (s, 36 H, *o-t*-Bu), 7.07 (m, 4 H, *m*-H). Raman (633 nm, 15 s, 10 scans, cm⁻¹): $\tilde{\nu}$ = 3075 (1), 2963 (2), 2924 (2), 2903 (3), 2863 (1), 2777 (1), 2709 (1), 1588 (1), 1527 (1), 1473 (1), 1461 (1), 1442 (1), 1396 (1), 1365 (1), 1292 (1), 1281 (1), 1241 (1), 1208 (1), 1201 (1), 1175 (1), 1152 (1), 1128 (1), 1033 (2), 1020 (1), 934 (1), 921 (1), 891 (1), 822 (2), 775 (1), 637 (1), 592 (10), 563 (1), 490 (1), 475 (1), 463 (1), 447 (1), 432 (1), 412 (1), 387 (1), 351 (4), 294 (1), 259 (2), 211 (1), 191 (1), 177 (1), 136 (1), 125 (2), 107 (3), 86 (3).

Synthesis of 5b

Method 1: HOTf (180 mg, 1.12 mmol) is condensed onto a degassed solution of Mes*PPN(i-Pr)₂ (489 mg, 1.12 mmol) in CH₂Cl₂ (8 mL) at -196 °C. The reaction mixture is slowly warmed to ambient temperature overnight. The solvent is removed *in vacuo* and the residue is extracted with *n*-hexane (5 mL). Insoluble solids are filtered off. The clear orange filtrate is concentrated, resulting in crystallization of a mixture of *exo-exo* and *endo-exo*-Mes*P₄Mes* (1 : 4 ratio). Yield: 120 mg (0.20 mmol, 35%). Re-crystallization yields pure *endo-exo*-Mes*P₄Mes*. Method 2: A mixture of [ClP(μ-PMes*)]₂ (835 mg, 1.22 mmol) and Me₄C₃N₂ (302 mg, 2.44 mmol) is dissolved in CH₂Cl₂ (10 mL) at -80 °C, resulting in a dark red solution. The reaction vessel is warmed to ambient temperature over a period of one hour, whereupon the solution is concentrated and stored at 5 °C, resulting in the crystallization of orange, block shaped crystals that were identified as Mes*PPMes*. The supernatant is separated and concentrated. Storage at 5 °C affords large colourless crystals of *endo-exo*-Mes*P₄Mes*. Yield: 105 mg (0.17 mmol, 14%). CHN calc. (found) in %: C 70.34 (70.04), H 9.51 (9.47). ³¹P{¹H} NMR (CD₂Cl₂, 121.5 MHz): δ = -220.4 (dd, ¹J_{AX}(³¹P,³¹P) = -234 Hz, ¹J_{AM}(³¹P,³¹P) = -213 Hz, 2 P, P_{bh}), -94.8 (td, ¹J_{AM}(³¹P,³¹P) = -213 Hz, ²J_{MX}(³¹P,³¹P) = -27 Hz, 1 P, P_{exo}), -54.7 (td, ¹J_{AX}(³¹P,³¹P) = -234 Hz, ²J_{MX}(³¹P,³¹P) = -27 Hz, 1 P, P_{endo}). ¹H NMR (CD₂Cl₂, 300.1 MHz): δ = 1.19 (s, 9 H, *exo*-Mes*, *p-t*-Bu), 1.30 (s, 9 H, *endo*-Mes*, *p-t*-Bu), 1.49 (s, 18 H, *exo*-Mes*, *o-t*-Bu), 1.66 (m, 18 H, *endo*-Mes*, *o-t*-Bu), 7.02 (m, 2 H, *exo*-Mes*, *m*-H), 7.05 (m, 2 H, *endo*-Mes*, *m*-H). Raman (633 nm, 15 s, 20 scans, cm⁻¹): $\tilde{\nu}$ = 3168 (1), 3074 (1), 3055 (1), 2959 (4), 2924 (4), 2902 (5), 2865 (2), 2778 (1), 2712 (1), 1584 (3), 1520 (1), 1475 (1), 1466 (2), 1444 (2), 1399 (1), 1392 (1), 1360 (1), 1283 (2), 1251 (1), 1203 (1), 1186 (1), 1182 (1), 1173 (1), 1148 (1), 1132 (2), 1033 (3), 1017 (2), 932 (1), 919 (2), 897 (1), 877 (1), 822 (4), 772 (1), 744 (1), 740 (1), 647 (1), 638 (1), 591 (2), 584 (2), 568 (10), 500 (2), 490 (1), 473 (1), 435 (1), 419 (2), 412 (2), 381 (4), 363 (2), 330 (1),



309 (1), 295 (1), 256 (2), 200 (1), 177 (1), 143 (4), 139 (3), 103 (7), 78 (6).

Synthesis of 5a-GaCl₃

Method 1: Solutions of PCl₃ (130 mg, 0.95 mmol) and GaCl₃ (168 mg, 0.95 mmol) in *n*-hexane (2 mL each) are added consecutively to a stirred solution of Mes*P(SiMe₃)₂ (403 mg, 0.95 mmol) in *n*-hexane (5 mL) at -80 °C. The mixture is warmed to ambient temperature, resulting in the deposition of an intensively red oil. Overnight, large colourless crystals grow at the phase interface at ambient temperature. Yield: 45 mg (0.07 mmol, 8%). Method 2: A solution of GaCl₃ (10 mg, 0.057 mmol) in CH₂Cl₂ (1 mL) is added to a solution of *exo-exo*-Mes*P₄Mes* (35 mg, 0.057 mmol) in CH₂Cl₂ (2 mL). The mixture is stirred for ten minutes and the solvent is removed *in vacuo*, yielding an analytically pure powder of *exo-exo*-Mes*P₄Mes*.GaCl₃. Yield: 30 mg (0.038 mmol, 67%). CHN calc. (found) in %: C 54.68 (53.97), H 7.39 (6.89). ³¹P{¹H} NMR (CD₂Cl₂, 121.5 MHz): δ = -246.4 (t, ¹J_{AX}(³¹P,³¹P) = -198 Hz, 2 P, P_{bridgehead}), -97.1 (broad, 2 P, PMes*). ³¹P{¹H} NMR (CD₂Cl₂, 121.5 MHz, -80 °C): δ = -248.1 (dd, ¹J_{AM}(³¹P,³¹P) = -182 Hz, ¹J_{AX}(³¹P,³¹P) = -216 Hz, 2 P, P_{bridgehead}), -114.0 (dt, ¹J_{AM}(³¹P,³¹P) = -182 Hz, ²J_{MX}(³¹P,³¹P) = +225 Hz, 1 P, PMes*), -74.8 (dt, ¹J_{AX}(³¹P,³¹P) = -216 Hz, ²J_{MX}(³¹P,³¹P) = +225 Hz, 1 P, P(Ga)Mes*). ¹H NMR (CD₂Cl₂, 300.1 MHz): δ = 1.20 (s, 18 H, Mes*, *p*-*t*-Bu), 1.68 (s, 36 H, *o*-*t*-Bu), 7.24 (s, 4 H, *m*-H). Raman (785 nm, 30 s, 4 scans, cm⁻¹): $\tilde{\nu}$ = 3064 (1), 2976 (1), 2960 (2), 2928 (2), 2904 (3), 2869 (1), 2786 (1), 2717 (1), 1593 (3), 1582 (2), 1536 (1), 1477 (2), 1465 (3), 1443 (2), 1393 (2), 1362 (1), 1284 (3), 1250 (2), 1208 (2), 1176 (3), 1031 (3), 1025 (3), 1016 (2), 920 (2), 891 (1), 819 (5), 772 (1), 747 (1), 638 (1), 613 (3), 597 (9), 561 (4), 502 (1), 497 (1), 480 (2), 470 (1), 451 (2), 436 (2), 406 (3), 395 (4), 385 (3), 366 (4), 343 (10), 294 (2), 260 (4).

Synthesis of 5b-GaCl₃

Method 1: A solution of PCl₃ (131 mg, 0.95 mmol) in CH₂Cl₂ (1 mL) and a solution of GaCl₃ (168 mg, 0.95 mmol) in CH₂Cl₂/toluene (1:1, 2 mL) are added consecutively to a stirred solution of Mes*P(SiMe₃)₂ (403 mg, 0.95 mmol) in CH₂Cl₂ (5 mL) at -80 °C. The mixture is warmed to -50 °C, whereupon the solution turns red. After further stirring at -50 °C for two hours, the solution is concentrated and subsequently warmed to ambient temperature overnight, resulting in crystallization of *endo-exo*-Mes*P₄Mes*.GaCl₃ (CH₂Cl₂ solvate) in colourless, block-shaped crystals. The solvent is removed by drying *in vacuo*. Yield: 50 mg (0.08 mmol, 9%). Method 2: A solution of GaCl₃ (15 mg, 0.085 mmol) in CH₂Cl₂ (1 mL) is added to a solution of *endo-exo*-Mes*P₄Mes* (52 mg, 0.085 mmol) in CH₂Cl₂ (2 mL). The mixture is stirred for ten minutes and the solvent is removed *in vacuo*, yielding an analytically pure powder of *endo-exo*-Mes*P₄Mes*.GaCl₃. Yield: 51 mg (0.064 mmol, 75%). CHN calc. (found) in %: C 54.68 (54.15), H 7.39 (7.15). ³¹P{¹H} NMR (CD₂Cl₂, 121.5 MHz): δ = -224.5 (dd, ¹J_{AM}(³¹P,³¹P) = -192 Hz, ¹J_{AX}(³¹P,³¹P) = -249 Hz, 2 P, P_{bridgehead}), -114.5 (td, ¹J_{AM}(³¹P,³¹P) = -192 Hz, ¹J_{MX}(³¹P,³¹P) = +24 Hz, 1 P, P_{exo}), -50.0 (broad, 1 P, P_{endo}). ¹H NMR (CD₂Cl₂,

300.1 MHz): δ = 1.21 (s, 9 H, *exo*-Mes*, *p*-*t*-Bu), 1.33 (s, 9 H, *endo*-Mes*, *p*-*t*-Bu), 1.49 (s, 18 H, *exo*-Mes*, *o*-*t*-Bu), 1.70 (m 18 H, *endo*-Mes*, *o*-*t*-Bu), 7.11 (d, $J(^1\text{H}, ^{31}\text{P}) = 1.9$ Hz, 2 H, *exo*-Mes*, *m*-H), 7.32 (d, $J(^1\text{H}, ^{31}\text{P}) = 5.0$ Hz, 2 H, *endo*-Mes*, *m*-H). Raman (633 nm, 10 s, 4 scans, cm⁻¹): $\tilde{\nu}$ = 3055 (2), 3035 (1), 2973 (5), 2966 (6), 2905 (7), 2866 (3), 2782 (1), 2714 (1), 1603 (1), 1582 (4), 1525 (1), 1463 (2), 1441 (2), 1394 (1), 1362 (1), 1284 (2), 1208 (2), 1173 (1), 1133 (2), 1029 (3), 1011 (2), 1002 (3), 924 (1), 818 (3), 784 (2), 741 (2), 618 (3), 567 (7), 518 (1), 508 (1), 438 (3), 407 (2), 391 (2), 372 (2), 348 (10), 302 (1), 258 (3), 213 (1).

Detailed analytical data for all compounds, including low temperature NMR data, can be found in the ESI.†

Acknowledgements

We thank Dr Dirk Michalik for the measurement of low-temperature NMR spectra, Dr Alexander Hinz for a gift of tetramethylimidazolyliene, and the Fonds der Chemischen Industrie (JB) as well as the Deutsche Forschungsgemeinschaft (SCHU 1170/11-1) for financial support.

Notes and references

- 1 L. Stahl, *Coord. Chem. Rev.*, 2000, **210**, 203–250.
- 2 M. S. Balakrishna, D. J. Eisler and T. Chivers, *Chem. Soc. Rev.*, 2007, **36**, 650–664.
- 3 G. He, O. Shynkaruk, M. W. Lui and E. Rivard, *Chem. Rev.*, 2014, **114**, 7815–7880.
- 4 O. J. Scherer, *Comments Inorg. Chem.*, 1987, **6**, 1–22.
- 5 M. Baudler and K. Glinka, *Chem. Rev.*, 1993, **93**, 1623–1667.
- 6 M. Scheer, G. Balázs and A. Seitz, *Chem. Rev.*, 2010, **110**, 4236–4256.
- 7 B. M. Cossairt, N. A. Piro and C. C. Cummins, *Chem. Rev.*, 2010, **110**, 4164–4177.
- 8 N. A. Giffin and J. D. Masuda, *Coord. Chem. Rev.*, 2011, **255**, 1342–1359.
- 9 J. D. Masuda, W. W. Schoeller, B. Donnadiou and G. Bertrand, *Angew. Chem., Int. Ed.*, 2007, **46**, 7052–7055.
- 10 S. Heintl, S. Reisinger, C. Schwarzmaier, M. Bodensteiner and M. Scheer, *Angew. Chem., Int. Ed.*, 2014, **53**, 7639–7642.
- 11 S. Heintl and M. Scheer, *Chem. Sci.*, 2014, **5**, 3221–3225.
- 12 J. E. Borger, A. W. Ehlers, M. Lutz, J. C. Sloatweg and K. Lammertsma, *Angew. Chem., Int. Ed.*, 2014, **53**, 12836–12839.
- 13 E. Niecke, R. Rieger and B. Krebs, *Angew. Chem., Int. Ed. Engl.*, 1982, **21**, 544–545.
- 14 A. H. Cowley, P. C. Knueppel and C. M. Nunn, *Organometallics*, 1989, **8**, 2490–2492.
- 15 H.-P. Schrödel, H. Nöth, M. Schmidt-Amelunxen, W. W. Schoeller and A. Schmidpeter, *Chem. Ber.*, 1997, **130**, 1801–1805.
- 16 P. Jutzi and T. Wippermann, *J. Organomet. Chem.*, 1985, **287**, C5–C7.



- 17 P. Jutzi and U. Meyer, *J. Organomet. Chem.*, 1987, **333**, C18–C20.
- 18 P. Jutzi, R. Kroos, A. Müller and M. Penk, *Angew. Chem.*, 1989, **101**, 628–629.
- 19 P. Jutzi and N. Brusdeilins, *Z. Anorg. Allg. Chem.*, 1994, **620**, 1375–1380.
- 20 L. Weber, G. Meine, R. Boese and N. Niederprün, *Z. Naturforsch., B: Chem. Sci.*, 1988, **43**, 415–721.
- 21 V. D. Romanenko, V. L. Rudzevich, E. B. Rusanov, A. N. Chernega, A. Senio, J.-M. Sotiropoulos, G. Pfister-Guilouzo and M. Sanchez, *J. Chem. Soc., Chem. Commun.*, 1995, 1383–1385.
- 22 R. Riedel, H.-D. Hausen and E. Fluck, *Angew. Chem., Int. Ed. Engl.*, 1985, **24**, 1056–1057.
- 23 E. Fluck, R. Riedel, H.-D. Hausen and G. Heckmann, *Z. Anorg. Allg. Chem.*, 1987, **551**, 85–94.
- 24 M. Baudler, C. Adamek, S. Opiela, H. Budzikiewicz and D. Ouzounis, *Angew. Chem., Int. Ed. Engl.*, 1988, **27**, 1059–1061.
- 25 M. Baudler and B. Wingert, *Z. Anorg. Allg. Chem.*, 1992, **611**, 50–55.
- 26 M. B. Power and A. R. Barron, *Angew. Chem., Int. Ed. Engl.*, 1991, **30**, 1353–1354.
- 27 A. R. Fox, R. J. Wright, E. Rivard and P. P. Power, *Angew. Chem., Int. Ed.*, 2005, **44**, 7729–7733.
- 28 I. Krossing and I. Raabe, *Angew. Chem., Int. Ed.*, 2001, **40**, 4406–4409.
- 29 M. H. Holthausen and J. J. Weigand, *J. Am. Chem. Soc.*, 2009, **131**, 14210–14211.
- 30 J. J. Weigand, M. H. Holthausen and R. Fröhlich, *Angew. Chem., Int. Ed.*, 2009, **48**, 295–298.
- 31 D. Holschumacher, T. Bannenberg, K. Ibrom, C. G. Daniliuc, P. G. Jones and M. Tamm, *Dalton Trans.*, 2010, **39**, 10590–10592.
- 32 S. Khan, R. Michel, J. M. Dieterich, R. A. Mata, H. W. Roesky, J. P. Demers, A. Lange and D. Stalke, *J. Am. Chem. Soc.*, 2011, **133**, 17889–17894.
- 33 J.-P. Bezombes, P. B. Hitchcock, M. F. Lappert and J. E. Nycz, *Dalton Trans.*, 2004, 499–501.
- 34 N. A. Giffin, A. D. Hendsbee, T. L. Roemmele, M. D. Lumsden, C. C. Pye and J. D. Masuda, *Inorg. Chem.*, 2012, **51**, 11837–11850.
- 35 C. Rotter, M. Schuster and K. Karaghiosoff, *Inorg. Chem.*, 2009, **48**, 7531–7533.
- 36 A. Sidiropoulos, B. Osborne, A. N. Simonov, D. Dange, A. M. Bond, A. Stasch and C. Jones, *Dalton Trans.*, 2014, **43**, 14858–14864.
- 37 M. Baudler and B. Wingert, *Z. Anorg. Allg. Chem.*, 1993, **619**, 1977–1983.
- 38 P. Jutzi, N. Brusdeilins, H.-G. Stammer and B. Neumann, *Chem. Ber.*, 1994, **127**, 997–1001.
- 39 O. J. Scherer, G. Schwarz and G. Wolmershäuser, *Z. Anorg. Allg. Chem.*, 1996, **622**, 951–957.
- 40 O. J. Scherer, T. Hilt and G. Wolmershäuser, *Organometallics*, 1998, **17**, 4110–4112.
- 41 P. Barbaro, C. Bazzicalupi, M. Peruzzini, S. Seniori Costantini and P. Stoppioni, *Angew. Chem., Int. Ed.*, 2012, **51**, 8628–8631.
- 42 S. Pelties, D. Herrmann, B. de Bruin, F. Hartl and R. Wolf, *Chem. Commun.*, 2014, 7014–7016.
- 43 N. Wiberg, A. Wörner, H.-W. Lerner and K. Karaghiosoff, *Z. Naturforsch., B: Chem. Sci.*, 2002, **57**, 1027–1035.
- 44 M. Donath, E. Conrad, P. Jerabek, G. Frenking, R. Fröhlich, N. Burford and J. J. Weigand, *Angew. Chem., Int. Ed.*, 2012, **51**, 2964–2967.
- 45 J. Bresien, K. Faust, A. Schulz and A. Villinger, *Angew. Chem., Int. Ed.*, 2015, **54**, 6926–6930.
- 46 J. Bresien, C. Hering, A. Schulz and A. Villinger, *Chem. – Eur. J.*, 2014, **20**, 12607–12615.
- 47 M. Yoshifuji, I. Shima, N. Inamoto, K. Hirotsu and T. Higuchi, *J. Am. Chem. Soc.*, 1981, **103**, 4587–4589.
- 48 M. Yoshifuji, I. Shima, N. Inamoto, K. Hirotsu and T. Higuchi, *J. Am. Chem. Soc.*, 1982, **104**, 6167.
- 49 Y. M. Bosworth, R. J. H. Clark and D. M. Rippon, *J. Mol. Spectrosc.*, 1973, **46**, 240–255.
- 50 P. Pyykkö and M. Atsumi, *Chem. – Eur. J.*, 2009, **15**, 12770–12779.
- 51 E. D. Glendening, J. K. Badenhop, A. E. Reed, J. E. Carpenter, J. A. Bohmann, C. M. Morales, C. R. Landis and F. Weinhold, *NBO 6.0*, Theoretical Chemistry Institute, University of Wisconsin, Madison, 2013.
- 52 T. Beweries, R. Kuzora, U. Rosenthal, A. Schulz and A. Villinger, *Angew. Chem., Int. Ed.*, 2011, **50**, 8974–8978.
- 53 H. Schmidbaur, A. Shiotani and H. F. Klein, *J. Am. Chem. Soc.*, 1971, **93**, 1555–1557.
- 54 J. B. DeRoos and J. P. Oliver, *J. Am. Chem. Soc.*, 1967, **89**, 3970–3977.

